

---

# Tetraphenylphosphonium as a Novel Molecular Probe for Imaging Tumors

Jung-Jun Min, MD, PhD; Sandip Biswal, MD; Christophe Deroose, MD; and Sanjiv S. Gambhir, MD, PhD

*Department of Radiology and the Bio-X Program, Stanford University School of Medicine, Stanford, California*

---

Mitochondrial membrane potential ( $\Delta\Psi_m$ )-dependent enhanced uptake of phosphonium salts, including  $^3\text{H}$ -tetraphenylphosphonium ( $^3\text{H}$ -TPP), in tumor cells, suggests the potential use of phosphonium salts as tracers for tumor imaging. In this study, we characterize the tumor accumulation of  $^3\text{H}$ -TPP and compare it with  $^{18}\text{F}$ -FDG in cell culture and in xenograft, metastatic, and inflammation models in living animals. **Methods:**  $^3\text{H}$ -TPP and  $^3\text{H}$ -FDG accumulation was compared in cell culture with a variety of cell lines in different glucose concentrations. Normal biodistribution and tumor uptake were assessed using nude mice with or without subcutaneous xenograft tumors (C6). To compare the accumulation of  $^3\text{H}$ -TPP and  $^{18}\text{F}$ -FDG in a metastatic tumor, severe combined immunodeficiency mice were tail-vein injected with human melanoma cell lines (A375-FL). To characterize the accumulation of  $^3\text{H}$ -TPP and  $^{18}\text{F}$ -FDG in inflammation, an inflammatory reaction was induced by subcutaneous injection of Complete Freund's Adjuvant in the left hind paw of Sprague-Dawley rat. **Results:** The  $\Delta\Psi_m$  data from a separate study and the current  $^3\text{H}$ -TPP uptake data showed good correlation ( $r^2 = 0.82$ ,  $P < 0.05$ ).  $^3\text{H}$ -TPP accumulation was significantly greater than that of  $^3\text{H}$ -FDG for glucose  $\geq 100$  mg/dL. The biodistribution study of  $^3\text{H}$ -TPP showed low uptake in most tissues but high accumulation in the heart and kidneys.  $^3\text{H}$ -TPP accumulation in xenograft or metastatic tumors was comparable with that of  $^{18}\text{F}$ -FDG, whereas  $^3\text{H}$ -TPP accumulation in inflammatory tissues was markedly lower than that of  $^{18}\text{F}$ -FDG. **Conclusion:** The sensitive tumor accumulation of  $^3\text{H}$ -TPP with less propensity for inflammatory regions warrants further investigation of radiolabeled phosphonium analogs for tumor imaging in living subjects.

**Key Words:** mitochondrial membrane potential; tetraphenylphosphonium; FDG; PET

**J Nucl Med 2004; 45:636–643**

---

**M**itochondria are central to cell life and death; therefore, it is not surprising that mitochondrial damage contributes to a wide range of diseases, including cancers, diabetes, degenerative diseases, and the pathophysiology of aging (1). The mitochondrial membrane potential ( $\Delta\Psi_m$ ) is higher in carcinoma cells than in normal epithelial cells (2–6). Li-

pophilic cations, including the fluorescent dye rhodamine-123 (Rh123) and tetraphenylphosphonium (TPP) salts, penetrate the hydrophobic barriers of the plasma and mitochondrial membranes and accumulate in mitochondria in response to the negative inner transmembrane potentials ( $-150$  to  $-170$  mV, negative inside) (4,6). The difference in  $\Delta\Psi_m$  between normal epithelial cells and carcinoma cells is at least 60 mV (5). In accordance with the Nernst equation, the 60 mV difference in membrane potential between carcinoma and control epithelial cells is sufficient to account for a 10-fold greater accumulation of the compound in carcinoma mitochondria (6). Thus, the development of radiolabeled phosphonium cations as a noninvasive imaging agent may serve as a new molecular “voltage sensor” probe to investigate the role of mitochondria in the pathophysiology and treatment of cancer.

$^{18}\text{F}$ -FDG, the most successful molecular probe in oncology available for routine use in the nuclear medicine clinic, is highly sensitive to malignancy (7) but is of limited specificity due to the enhanced accumulation in inflammation, in granulomatous diseases, and in autoimmune diseases (8–10). Uptake studies in varying cell lines indicate that  $\Delta\Psi_m$  of immune cells is relatively lower (11), whereas that of malignant cells is greater than normal epithelial cells, suggesting that  $^3\text{H}$ -TPP may have an advantage over  $^{18}\text{F}$ -FDG for differentiation of tumor from inflammation. In this study, we report tumor-specific uptake of  $^3\text{H}$ -TPP that accumulates highly in malignant neoplasms but very minimally in an adjuvant inflammatory tissue.

## MATERIALS AND METHODS

### Radiolabeled Compounds, Cell Lines, Culture Conditions, and Cell Uptake Studies

$^3\text{H}$ -TPP (1.11 TBq/mmol [30 Ci/mmol]) and  $^3\text{H}$ -FDG 2.22 TBq/mmol ([60 Ci/mmol]) were purchased from Moravek Biochemicals, Inc.  $^{18}\text{F}$ -FDG was synthesized by the method described by Hamacher et al. (12) at a specific activity of  $\approx 185$  TBq/mmol ( $\approx 5,000$  Ci/mmol).

$^3\text{H}$ -TPP and  $^3\text{H}$ -FDG accumulation was compared in cell culture with 9 cell lines: rat glioma (C6), human cervix cancer (HeLa), human melanoma (K1735), human breast cancer (MCF7), rat Morris hepatoma (MH3924A), human bronchioalveolar carcinoma (A549), human prostate cancer (LnCap), human tongue cancer (SCC-15), and mouse neuroblastoma (N2A)

---

Received Nov. 7, 2003; revision accepted Dec. 4, 2003.

For correspondence contact: Sanjiv S. Gambhir, MD, PhD, The James H. Clark Center, 318 Campus Dr., East Wing, First Floor, Stanford, CA 94305-5427.

E-mail: sgambhir@stanford.edu

cell lines. C6 cells were grown in Deficient DMEM (Dulbecco's modified Eagle medium) High Glucose (containing KCl 5.3 mmol/L and NaCl 110.34 mmol/L; Life Technologies) plus 5% fetal bovine serum (FBS), 1% penicillin-streptomycin, and 1% L-glutamine; HeLa, SCC-15, K1735, and N2A cells were grown in DMEM High Glucose (containing KCl 5.3 mmol/L and NaCl 110.34 mmol/L) plus 10% FBS and 1% penicillin-streptomycin; MH3924A cells were grown in RPMI 1640 medium (containing KCl 5.3 mmol/L and NaCl 103.44 mmol/L; Life Technologies) plus 20% fetal calf serum (FCS) and 1% penicillin-streptomycin; A549 cells were grown in RPMI 1640 medium plus 10% FCS and 1% penicillin-streptomycin; and MCF7 and LnCap cells were grown in RPMI 1640 medium plus 10% FBS and 1% penicillin-streptomycin.

Uptake of  $^3\text{H}$ -TPP (37 kBq/mL [1.0  $\mu\text{Ci}$ /mL]) and  $^3\text{H}$ -FDG (37 kBq/mL [1.0  $\mu\text{Ci}$ /mL]) was directly compared in these cell lines. Cells were incubated at 37°C from 15 to 120 min with radioactive culture medium with  $^3\text{H}$ -TPP or  $^3\text{H}$ -FDG. To assess the effects of glucose concentration on the uptake of  $^3\text{H}$ -TPP and  $^3\text{H}$ -FDG, uptake studies were performed under 5 different glucose concentrations of culture media (0, 50, 100, 150, 200 mg/dL) using C6, HeLa, K1735, and MCF7 cells. At the end of each incubation period, radioactive medium was removed and radioactivity was measured. The wells were washed with cold phosphate-buffered saline, the cells were harvested using a cell scraper, and the cell-associated radioactivity was determined. Triplicate samples were obtained for all uptake studies. Data are expressed as the normalized accumulation of probe in (dpm cells/dpm medium/ $\mu\text{g}$  total protein)  $\pm$  SE.  $^3\text{H}$  analyses were performed with a Beckman LS-6500 liquid scintillation counter with Biosafe II scintillation fluid (Research Products International). The disintegration per minute (dpm) was obtained by correcting for background activity and efficiency (69.3% for  $^3\text{H}$ ).

We assessed the correlation between  $^3\text{H}$ -TPP uptake from this study and  $\Delta\Psi\text{m}$  data from previously published results (2) in HeLa, LnCap, MCF7, A549, N2A, SCC-15, and K1735 cell lines. The  $\Delta\Psi\text{m}$  has been measured by Rh123 retention and expressed as a percentage of Rh123 retention in diverse tumor cells relative to retention in rat cardiac muscle cells. The detailed methods are described elsewhere (2).

### Animal Studies

To compare the uptake of  $^{18}\text{F}$ -FDG and  $^3\text{H}$ -TPP in tumors and inflammatory tissues, we performed microPET studies, digital whole-body autoradiography (DWBA), and biodistribution studies with a murine model with or without a subcutaneous xenograft tumor, metastatic lesions, or an inflammatory lesion. Animal care and euthanasia were performed with the approval of the University of California Animal Research Committee.

To establish the subcutaneous xenografts, 10- to 12-wk-old male nude mice (*nu/nu*,  $\approx 25$  g; Charles River Laboratories, Inc.) were subcutaneously injected with  $1 \times 10^6$  C6 cells on the left shoulder ( $n = 10$ ). Tumor uptake studies were performed using nude mice carrying subcutaneous xenografts using DWBA ( $n = 2$ ) and biodistribution studies ( $n = 8$ ) (7.4 MBq [200  $\mu\text{Ci}$ ]  $^{18}\text{F}$ -FDG and 370 kBq [10  $\mu\text{Ci}$ ]  $^3\text{H}$ -TPP). Before injecting  $^{18}\text{F}$ -FDG, mice were restricted from foods for at least 4 h and anesthetized by intraperitoneal injection of  $\approx 30$   $\mu\text{L}$  of a ketamine-xylazine (4:1) solution. Biodistribution of  $^3\text{H}$ -TPP and  $^{18}\text{F}$ -FDG in different organs of 12 nude mice was also assessed by coinjecting 7.4 MBq (200  $\mu\text{Ci}$ )  $^{18}\text{F}$ -FDG and 370 kBq (10  $\mu\text{Ci}$ )  $^3\text{H}$ -TPP via tail vein.

To develop a metastatic tumor model, severe combined immune deficiency (SCID) mice ( $\approx 28$  g; Charles River Breeding Laboratories) were tail-vein injected with human melanoma cell lines stably expressing firefly luciferase (A375-FL;  $5 \times 10^5$ ). The In Vivo Imaging System (IVIS; Xenogen) with a cooled charge-coupled device (CCD) camera was used to noninvasively and repetitively monitor the metastatic lesions. Biodistribution studies ( $n = 6$ ) were performed after injection of 7.4 MBq (200  $\mu\text{Ci}$ )  $^{18}\text{F}$ -FDG and 370 kBq (10  $\mu\text{Ci}$ )  $^3\text{H}$ -TPP via tail vein.

To characterize the accumulation of  $^3\text{H}$ -TPP and  $^{18}\text{F}$ -FDG in inflammation, an inflammatory reaction was induced by subcutaneous injection of 50  $\mu\text{L}$  Complete Freund's Adjuvant ([CFA], inactivated *Mycobacterium tuberculosis*, 10 mg/mL) in the left hind paw of 6 Sprague-Dawley rats ( $\approx 250$ –300 g; Charles River Laboratories, Inc.) as previously described (13). The right hind paw was injected with physiologic saline as a negative control. Fourteen days after CFA injection, the rat received an intravenous injection of 74 MBq (2 mCi)  $^{18}\text{F}$ -FDG and 3.7 MBq (100  $\mu\text{Ci}$ )  $^3\text{H}$ -TPP. One hour later, the  $^{18}\text{F}$ -FDG microPET imaging study ( $n = 6$ ), autoradiography ( $n = 3$ ), and  $^3\text{H}$ -TPP autoradiography ( $n = 3$ ) were done.

### microPET Imaging Studies

Mice and rats were imaged using a microPET using  $^{18}\text{F}$ -FDG to image glucose viability of tumor or inflammatory lesions. Images were reconstructed using 3-dimensional filtered backprojection. Regions of interest (ROIs) were drawn over the tumor or inflammation area on decay-corrected whole-body coronal images. The counts per pixel per minute obtained from the ROI were converted to counts per milliliter per minute by using a calibration constant obtained from scanning a cylinder phantom in the microPET scanner. The ROI counts per milliliter per minute were converted to counts per gram per minute, assuming a tissue density of 1 g/mL, and divided by the injected dose (ID) to obtain an image ROI-derived percentage ID per gram of tissue (%ID/g). The details of microPET scanning and data analysis are described elsewhere (14).

### Optical Cooled CCD Camera Imaging

In vivo optical imaging for firefly luciferase (FL) was done 20 min after intraperitoneal injection of 3 mg of D-Luciferin per animal using a Xenogen-IVIS cooled CCD optical system (Xenogen) (15). Photons emitted from FL-expressing cells (A375-FL) injected via tail vein in the mice were collected and integrated for a period of 1 min. Images were obtained by superimposed gray-scale photographic images and FL color images using the overlay option of the Living Image software (Xenogen) and Igor Image analysis software (Wave Metrics).

### Murine Biodistribution Studies

Tissue biodistribution studies were performed with normal organs, tumor xenografts, or metastatic lesions. For the  $^{18}\text{F}$ -FDG biodistribution study, organs or tumors were removed and radioactivity was measured using a well counter (Cobra II Auto- $\gamma$ -Packard; Packard). For counting  $^3\text{H}$ -TPP radioactivity, tissue was dissolved overnight in 1 mL of tissue solubilizer (Sigma) and counted using a Beckman LS-6500 liquid scintillation counter. Radioactivity determinations were normalized by the weight of the tissue and the amount of radioactivity injected, to obtain the %ID/g. The details of  $^3\text{H}$  biodistribution are described elsewhere (16).

## DWBA

For imaging of  $^3\text{H}$ -TPP and  $^{18}\text{F}$ -FDG accumulation in tumors and inflammatory lesions, DWBA was performed. After killing, each animal was frozen in liquid nitrogen in preparation for DWBA using a 45- $\mu\text{m}$  slice thickness (14). The exposure time was 2–4 wk for  $^3\text{H}$  and 12–24 h for  $^{18}\text{F}$ . All digital plates were scanned on a Fuji BAS 5000 phosphorimager at resolution of  $\approx 100\ \mu\text{m}$ .

## Statistical Analysis

Comparisons between 2 groups were made using a Student  $t$  test for independent samples with unequal variances. Comparisons between 3 groups were made with a 1-way ANOVA. Values of  $P < 0.05$  were considered statistically significant. Linear regression analysis was performed to assess the linear relationship between the  $\Delta\Psi\text{m}$  data from previously published results (2) and the current  $^3\text{H}$ -TPP uptake data. The degree of correlation between them was quantified in terms of the square of Pearson product moment correlation coefficient ( $r^2$ ).

## RESULTS

### $^3\text{H}$ -TPP Accumulation Is Higher Than That of $^{18}\text{F}$ -FDG in Several Cancer Cell Lines in Cell Culture

We first performed  $^3\text{H}$ -TPP cell uptake studies in 7 different cancer cell lines from 15 to 120 min after exposure to  $^3\text{H}$ -TPP. Cellular uptake of  $^3\text{H}$ -TPP increased until 120 min in most of the cell lines, except for N2A, which showed the lowest uptake (data not shown). We also assessed the correlation between  $^3\text{H}$ -TPP uptake from this study and the  $\Delta\Psi\text{m}$  data from previously published results (2) in HeLa, LnCap, MCF7, A549, N2A, SCC-15, and K1735 cell lines. The  $\Delta\Psi\text{m}$  data and the current  $^3\text{H}$ -TPP uptake data showed good correlation (Fig. 1A;  $r^2 = 0.82$ ,  $P < 0.05$ ). Because uptake of  $^{18}\text{F}$ -FDG into the cell is affected by glucose concentration of culture media, we performed cellular uptake studies of  $^3\text{H}$ -FDG and  $^3\text{H}$ -TPP in different glucose

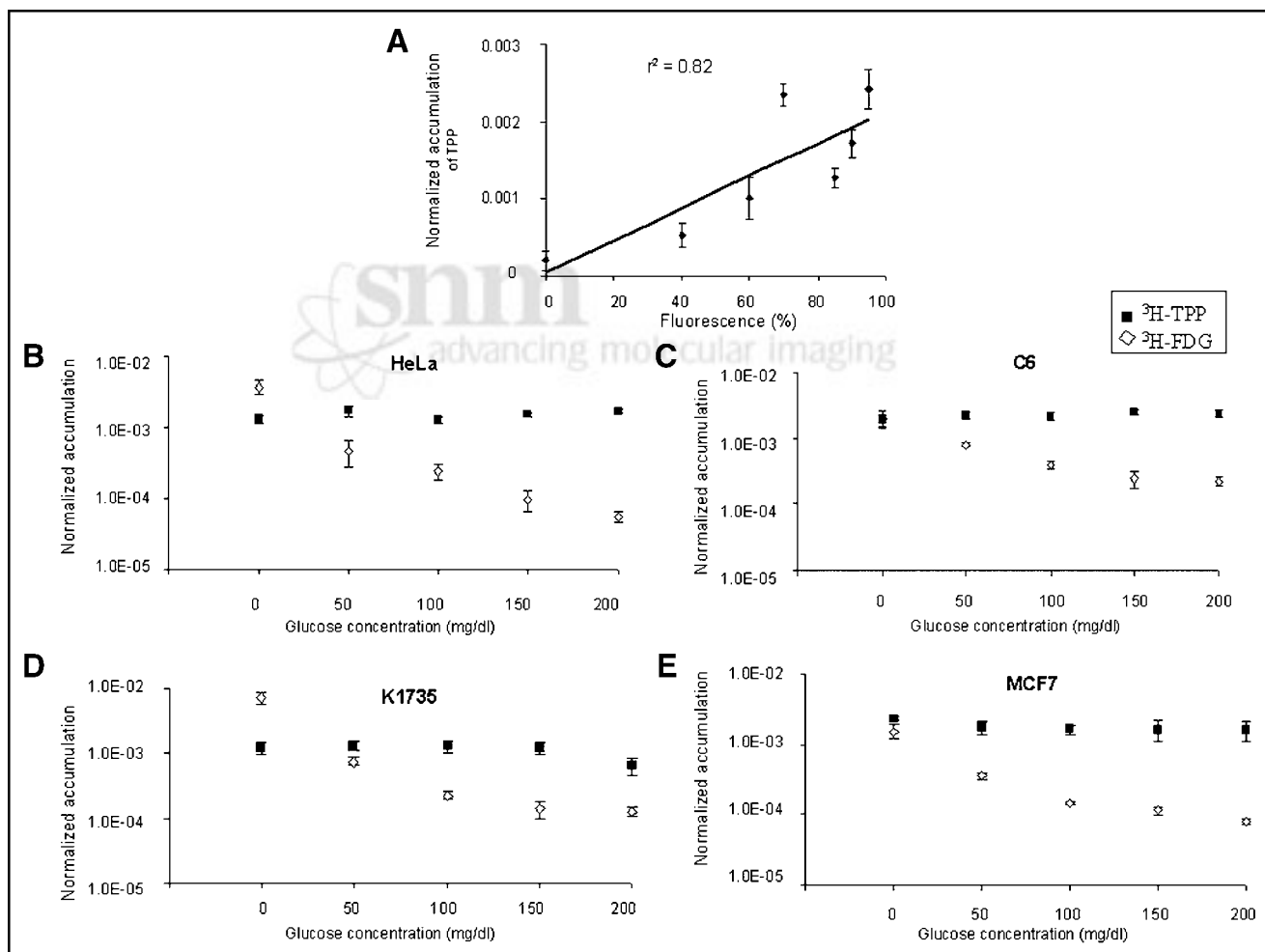


**FIGURE 1.** (A)  $\Delta\Psi\text{m}$  data (2) and current  $^3\text{H}$ -TPP uptake data showed good correlation ( $r^2 = 0.82$ ) in HeLa, LnCap, MCF7, A549, N2A, SCC-15, and K1735 cell lines.  $^3\text{H}$ -TPP accumulation data are expressed as normalized accumulation of probe in (dpm cells/dpm medium/ $\mu\text{g}$  total protein)  $\pm$  SE. (B–E)  $^3\text{H}$ -TPP significantly accumulates in HeLa (B), C6 (C), K1735 (D), and MCF7 (E) cell lines in cell culture. Cellular uptake studies with  $^3\text{H}$ -TPP and  $^3\text{H}$ -FDG were performed under 5 different glucose concentrations of culture media (0, 50, 100, 150, 200 mg/dL). Data are expressed as normalized accumulation of probe in (dpm cells/dpm medium/ $\mu\text{g}$  total protein)  $\pm$  SE. Though  $^3\text{H}$ -FDG accumulation in cell culture is dependent on medium glucose concentration,  $^3\text{H}$ -TPP accumulation is constant for all glucose concentrations.  $^3\text{H}$ -TPP accumulation is significantly ( $P < 0.05$ ) greater than that of  $^3\text{H}$ -FDG for glucose  $\geq 50$  mg/dL in C6, HeLa, and MCF7 cells.  $^3\text{H}$ -TPP accumulation is significantly ( $P < 0.05$ ) greater than that of  $^3\text{H}$ -FDG for glucose  $\geq 100$  mg/dL in K1735 cells.

concentrations of culture medium with HeLa, C6, K1735, and MCF7 cell lines (Figs. 1B–1E). Though  $^3\text{H}$ -FDG accumulation in cell culture was dependent on medium glucose concentration,  $^3\text{H}$ -TPP accumulation was relatively constant for all glucose concentrations tested.  $^3\text{H}$ -TPP accumulation was significantly ( $P < 0.01$ ) greater than that of  $^3\text{H}$ -FDG for glucose  $\geq 50$  mg/dL in C6, HeLa, and MCF7 cells and for glucose  $\geq 100$  mg/dL in K1735 cells.

### Biodistribution of $^3\text{H}$ -TPP Shows High Accumulation in Heart and Kidneys

We performed biodistribution studies for  $^3\text{H}$ -TPP (Fig. 2A) and  $^{18}\text{F}$ -FDG (Fig. 2B) for each tracer at 10, 30, 60, and 120 min after tail-vein injection ( $n = 12$ ). Normal biodistribution of  $^3\text{H}$ -TPP (Fig. 2A) showed high accumulation in the heart ( $8.3 \pm 1.4$  %ID/g at 1 h) and kidneys ( $17.8 \pm 3.5$  %ID/g at 1 h; Fig. 3) but low uptake in other tissues

(0.04–3.2 %ID/g at 1 h).  $^3\text{H}$ -TPP exhibited very low values in blood as early as 10 min, reflecting rapid washout from blood.  $^3\text{H}$ -TPP showed very low values in brain, which was similar to other cationic radiopharmaceuticals with poor blood–brain barrier permeability. Normal biodistribution of  $^{18}\text{F}$ -FDG (Fig. 2B) showed high accumulation in the heart ( $7.6 \pm 2.2$  %ID/g at 1 h) and kidneys ( $7.7 \pm 4.0$  %ID/g at 1 h). The radioactivity of  $^{18}\text{F}$ -FDG in the other organs was low (1.4–3.1 %ID/g at 1 h).

### $^3\text{H}$ -TPP Accumulation Is Not Statistically Different from That of $^{18}\text{F}$ -FDG in Xenograft and Metastatic Tumors

We subcutaneously implanted C6 cells in the mouse left shoulder to develop xenografts ( $n = 10$ ). When tumors reached 5–10 mm size, we performed DWBA ( $n = 2$ ) or biodistribution studies ( $n = 8$ ) using  $^3\text{H}$ -TPP and  $^{18}\text{F}$ -FDG. We also injected A375-FL cells via the tail vein of SCID

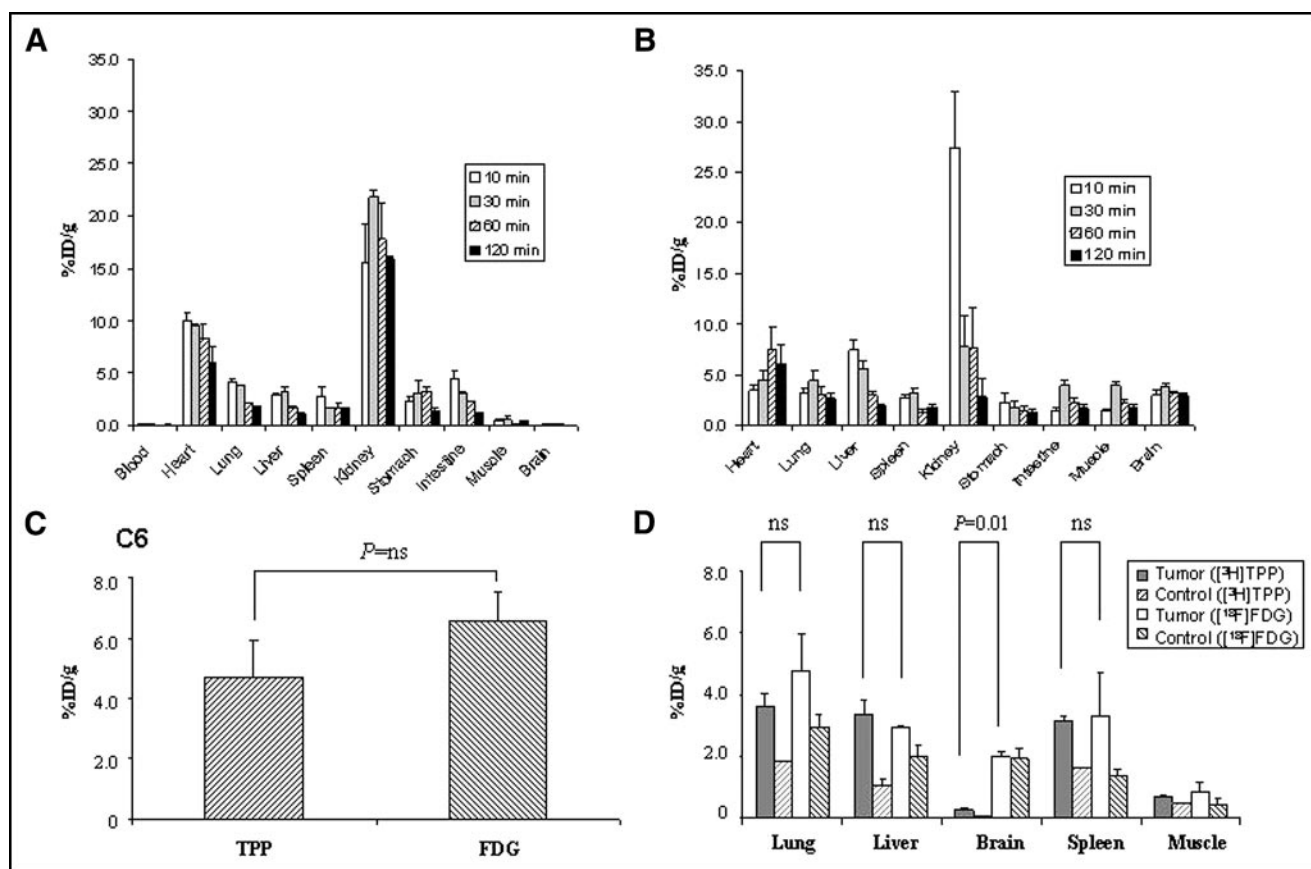


**FIGURE 2.** Biodistribution of  $^3\text{H}$ -TPP and  $^{18}\text{F}$ -FDG in normal nude mice and mouse models with tumor xenografts or metastases. (A) Biodistribution of  $^3\text{H}$ -TPP in normal nude mice ( $n = 12$ ) showed relatively high accumulation in heart ( $8.3 \pm 1.4$  %ID/g at 1 h) and kidneys ( $17.8 \pm 3.5$  %ID/g at 1 h) but low uptake in other tissues (0.04–3.2 %ID/g at 1 h).  $^3\text{H}$ -TPP exhibits very low values in blood as early as 10 min and in brain. (B) Biodistribution of  $^{18}\text{F}$ -FDG in different organs of nude mice ( $n = 12$ ) shows high accumulation in heart ( $7.6 \pm 2.2$  %ID/g at 1 h) and kidneys ( $7.7 \pm 4.0$  %ID/g at 1 h). Radioactivity of  $^{18}\text{F}$ -FDG in other organs is relatively low (1.4–3.1 %ID/g at 1 h). (C) Comparison of  $^3\text{H}$ -TPP and  $^{18}\text{F}$ -FDG accumulation in nude mice carrying xenograft tumor ( $n = 8$ ).  $^3\text{H}$ -TPP accumulation in C6 xenograft tumor ( $4.7 \pm 1.2$  %ID/g) is slightly lower than that of  $^{18}\text{F}$ -FDG ( $6.5 \pm 1.0$  %ID/g;  $P = \text{not significant [ns]}$ ). (D) Comparison of  $^3\text{H}$ -TPP and  $^{18}\text{F}$ -FDG accumulation in metastatic lesions of malignant melanoma in SCID mice ( $n = 6$ ).  $^3\text{H}$ -TPP vs.  $^{18}\text{F}$ -FDG accumulation in metastatic lung ( $3.6 \pm 0.4$  %ID/g vs.  $4.8 \pm 0.7$  %ID/g), liver ( $3.4 \pm 0.4$  %ID/g vs.  $2.9 \pm 0.1$  %ID/g), and spleen ( $3.2 \pm 0.1$  %ID/g vs.  $3.3 \pm 0.7$  %ID/g) is not significantly different.  $^{18}\text{F}$ -FDG accumulation in metastatic brain is significantly higher than that of  $^3\text{H}$ -TPP ( $2.0 \pm 0.2$  %ID/g vs.  $0.3 \pm 0.1$  %ID/g;  $P = 0.01$ ). All values are mean  $\pm$  SE.

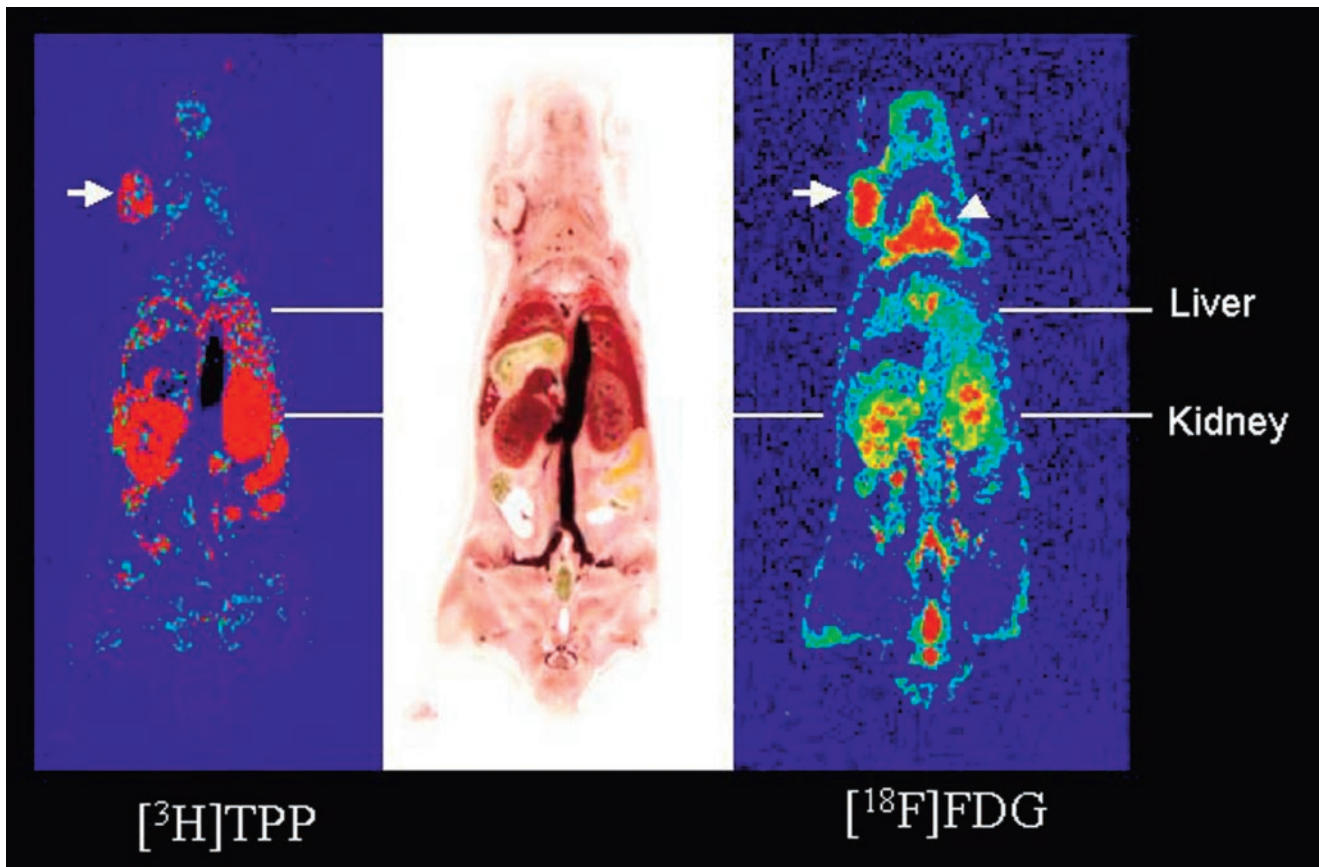


**FIGURE 3.** Autoradiographic images of  $^3\text{H}$ -TTP and  $^{18}\text{F}$ -FDG in C6 xenograft tumor. C6 cells were subcutaneously implanted in left shoulders of mice to develop xenograft tumor model. When tumors reached 8 mm of size, DWBA was performed with tail-vein injection of  $^3\text{H}$ -TTP (370 kBq [10  $\mu\text{Ci}$ ]) and  $^{18}\text{F}$ -FDG (7.4 MBq [200  $\mu\text{Ci}$ ]) using the same animal. (Left)  $^3\text{H}$ -TTP accumulation in C6 xenograft tumor (arrow). This image exhibits relatively low background radioactivity except for strong renal activity. (Right)  $^{18}\text{F}$ -FDG accumulation in C6 xenograft tumor (arrow).  $^{18}\text{F}$ -FDG uptake is observed in kidneys, blood vessels, and dorsal upper back, indicating brown adipose tissue (arrowhead). (Middle) Tissue section (45- $\mu\text{m}$  thickness) corresponding to DWBA images.

mice ( $n = 6$ ) to develop metastatic tumors. Tumor metastases were monitored by noninvasively observing the bioluminescence signal from internal organs.

$^3\text{H}$ -TTP accumulation in C6 xenograft tumors ( $4.7 \pm 1.2$  %ID/g) was somewhat lower but not statistically significant as compared with  $^{18}\text{F}$ -FDG ( $6.5 \pm 1.0$  %ID/g;  $P =$  not significant [ns]; Fig. 2C).  $^3\text{H}$ -TTP versus  $^{18}\text{F}$ -FDG accumulation in metastatic lung ( $3.6 \pm 0.4$  %ID/g vs.  $4.8 \pm 0.7$  %ID/g), metastatic liver ( $3.4 \pm 0.4$  %ID/g vs.  $2.9 \pm 0.1$  %ID/g), and metastatic spleen ( $3.2 \pm 0.1$  %ID/g vs.  $3.3 \pm 0.7$  %ID/g) was not significantly different ( $P =$  ns; Fig. 2D).  $^{18}\text{F}$ -FDG accumulation in metastatic brain was significantly higher than that of  $^3\text{H}$ -TTP ( $2.0 \pm 0.2$  %ID/g vs.  $0.3 \pm 0.1$  %ID/g;  $P = 0.01$ ). Although  $^3\text{H}$ -TTP accumulation was very low in the metastatic brain tumor, the metastatic-to-normal brain ratio was  $8.3 \pm 1.6$ , whereas that of  $^{18}\text{F}$ -FDG was  $1.03 \pm 0.1$  ( $P < 0.0001$ ). DWBA images showed high accumulation of both  $^3\text{H}$ -TTP and  $^{18}\text{F}$ -FDG in the C6 xenograft tumor (Fig. 3).  $^{18}\text{F}$ -FDG uptake was also observed in kidneys, liver, blood vessels, bladder, intestine, and dorsal upper back, indicating brown adipose tissue (BAT), whereas  $^3\text{H}$ -TTP activity was found in kidneys, liver, and intestine.

### $^3\text{H}$ -TTP Accumulation in Inflammatory Tissue Is Markedly Lower Than That of $^{18}\text{F}$ -FDG

We developed an inflammation model in the left hind paw of Sprague–Dawley rats ( $n = 6$ ) and tail-vein injected  $^3\text{H}$ -TTP and  $^{18}\text{F}$ -FDG to perform microPET ( $n = 6$ ) and autoradiographic studies ( $n = 3$ ), respectively. CFA pretreatment in the left hind paw as compared with the control right hind paw of rats caused a significant increase in  $^{18}\text{F}$ -FDG accumulation seen in both microPET images ( $2.1 \pm 0.3$  %ID/g vs.  $0.3 \pm 0.01$  %ID/g; ratio =  $7.2 \pm 0.6$ ) and autoradiography (Fig. 4). However, when  $^3\text{H}$ -TTP radioactivity of both hind paws was measured by using ImageReader software (Fuji),  $^3\text{H}$ -TTP showed very low accumulation in inflammatory tissue in autoradiography (ratio =  $1.1 \pm 0.2$ ).

### DISCUSSION

The major finding of this study was the tumor-specific uptake of  $^3\text{H}$ -TTP that accumulates highly in tumor tissues but very minimally in an adjuvant inflammatory tissue. The cell culture studies across various cell types clearly demonstrate that  $^3\text{H}$ -TTP accumulates in malignant cells greater

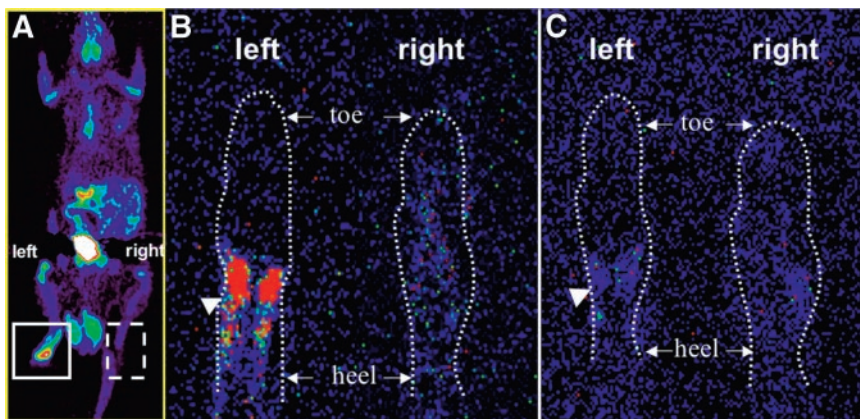


**FIGURE 4.** Comparison of  $^{18}\text{F}$ -FDG and  $^3\text{H}$ -TPP accumulation in inflammatory tissue. Inflammatory reaction was induced by subcutaneous injection of 50  $\mu\text{L}$  of CFA (10 mg/mL) in left hind paw of Sprague–Dawley rat. Right hind paw was injected with saline as negative control.  $^3\text{H}$ -TPP (3.7 MBq [100  $\mu\text{Ci}$ ]) and  $^{18}\text{F}$ -FDG (74 MBq [2 mCi]) were injected via tail vein to perform autoradiography and microPET studies, respectively. (A) Whole-body microPET image of Sprague–Dawley rat shows strong accumulation of  $^{18}\text{F}$ -FDG in inflammatory tissue of left hind paw. After killing the rat, autoradiographic studies for  $^{18}\text{F}$ -FDG and  $^3\text{H}$ -TPP were performed using the same animal. (B)  $^{18}\text{F}$ -FDG autoradiographic image of coronal section of inflammatory (left) and control (right) hind paw. CFA pretreatment in left hind paw as compared with control right hind paw (saline injected) of rat caused significant increase in  $^{18}\text{F}$ -FDG accumulation (arrowhead) corresponding to microPET image. (C)  $^3\text{H}$ -TPP autoradiographic image of coronal section of inflammatory (left) and control (right) hind paw. This slice was taken right after slice for  $^{18}\text{F}$ -FDG (45  $\mu\text{m}$ ).  $^3\text{H}$ -TPP shows very mild possible accumulation in inflammatory tissue of left hind paw (arrowhead).

than that of  $^{18}\text{F}$ -FDG at physiologically relevant glucose levels. C6, HeLa, and MCF7 cells show higher  $^3\text{H}$ -TPP accumulation than that of  $^{18}\text{F}$ -FDG at a glucose concentration of  $\geq 50$  mg/dL. The malignant melanoma cell line K1735, which strongly accumulates  $^{18}\text{F}$ -FDG, shows higher  $^3\text{H}$ -TPP accumulation than that of  $^{18}\text{F}$ -FDG at  $\geq 100$  mg/dL of glucose concentration. Results of animal studies with xenograft or metastatic tumor models demonstrate selective accumulation of  $^3\text{H}$ -TPP in tumor cells that is quite comparable to that of  $^{18}\text{F}$ -FDG. Although accumulation of  $^3\text{H}$ -TPP in brain metastases was significantly lower than that of  $^{18}\text{F}$ -FDG, the metastatic-to-normal brain ratio was significantly greater with  $^3\text{H}$ -TPP than with  $^{18}\text{F}$ -FDG ( $8.3 \pm 1.6$  vs.  $1.03 \pm 0.1$ ;  $P < 0.0001$ ).

In separate studies, increased  $\Delta\Psi_{\text{m}}$  has been assessed with lipophilic cations such as Rh123 and phosphonium salts. The results of a 6-y systematic study overwhelmingly indicate that all normal epithelial cells tested have low  $\Delta\Psi_{\text{m}}$ —hence, low Rh123 uptake and retention. In contrast, screening of 200 cells derived from tumors of kidney, ovary, pancreas, lung, adrenal cortex, skin, breast, prostate, cervix, vulva, colon, liver, testis, esophagus, trachea, and tongue show that a great majority of adenocarcinoma, transitional cell carcinoma, squamous cell carcinoma, and melanoma have high Rh123 uptake and retention (2,3). The most significant exceptions have been human oat cell and large cell carcinomas of lung and poorly differentiated carcinoma of the colon. High Rh123 uptake and retention have not been detected in leukemia, lymphoma, neuroblastoma, or osteosarcoma, (2–4). In specimens taken from patients with brain tumors,  $^3\text{H}$ -TPP accumulation in dispersed glioma cells was 40 times higher than that in normal

epithelial cells (17). Other studies provide evidence that radiolabeled phosphonium salts showed high tumor selectivity in the mouse model of non-small cell lung carcinoma (18) and in canine gliomas (19).

There has been extensive cell culture and in vivo tumor imaging experience with another lipophilic cation,  $^{99\text{m}}\text{Tc}$ -sestamibi (20). Uptake of this agent in tumor cells and the relation to membrane potential have been discussed and compared with  $^3\text{H}$ -TPP in an earlier publication (21). Depolarizing the plasma membrane potential in high  $\text{K}^+$  buffer resulted in all cases in lowering the uptake of  $^{99\text{m}}\text{Tc}$ -sestamibi in a manner similar to that of  $^3\text{H}$ -TPP. Furthermore, alteration of the  $\Delta\Psi_{\text{m}}$  induced significant variation of  $^{99\text{m}}\text{Tc}$ -sestamibi uptake, suggesting that the  $\Delta\Psi_{\text{m}}$  could also be a contributing factor. Recently,  $^3\text{H}$ -TPP and  $^{99\text{m}}\text{Tc}$ -sestamibi were directly compared in non-small cell lung carcinoma in mice (18).  $^3\text{H}$ -TPP exhibited a stronger accumulation in malignant tissue and a greater tumor-to-nontumor ratio than did  $^{99\text{m}}\text{Tc}$ -sestamibi.

Although uptake of the lipophilic cations such as TPP and Tc-sestamibi is sensitive to the  $\Delta\Psi_{\text{m}}$  in cell culture studies, lipophilic compounds also have a high first-pass extraction and retention and are strongly dependent on blood flow in vivo (22,23). Tumor uptake of TPP may be also influenced by enhanced blood flow compared with adjacent tissues with respect to the results of biodistribution studies showing some features of a blood flow agent: high early uptake and rapid blood clearance in most organs. It is assumed that initial uptake of TPP may be dependent on blood flow, whereas retention in mitochondria might depend on the  $\Delta\Psi_{\text{m}}$ . The kinetics of TPP will need to be further studied using dynamic PET studies with  $^{18}\text{F}$ - or  $^{11}\text{C}$ -TPP.

$^3\text{H}$ -TPP accumulation in inflammatory tissue was significantly lower than that of  $^{18}\text{F}$ -FDG in this study.  $^{18}\text{F}$ -FDG strongly accumulates at CFA-induced inflammatory tissues, whereas  $^3\text{H}$ -TPP shows very mild uptake. High  $^{18}\text{F}$ -FDG uptake is not specific to cancer but is also found in inflammatory lesions (8–10). This may reduce the diagnostic specificity of  $^{18}\text{F}$ -FDG PET in oncology. It has been reported that  $^{18}\text{F}$ -FDG uptake in inflammatory tissue is due to accumulation in inflammatory cells such as macrophages (9), lymphocytes (24), and granulocytes (25). It is commonly assumed that human immune cells such as neutrophils have a relatively lower  $\Delta\Psi\text{m}$  based on the fact that electron microscopy usually fails to identify intact mitochondria, and any that are seen are small with poorly defined cristae and inner mitochondrial membrane definition (11). An earlier study also exhibited very low Rh123 accumulation in lymphocytes, monocytes, and macrophages (2). The lower  $\Delta\Psi\text{m}$  of immune cells may be one of the causes of weak  $^3\text{H}$ -TPP accumulation in inflammatory tissues. This result suggests the possible role of radiolabeled phosphonium salts to differentiate malignant tumor from inflammation. Interestingly, a question arises: Why does TPP uptake not increase in inflammatory lesions in spite of evidence of increased blood flow? Because the  $\Delta\Psi\text{m}$  of immune cells is low, secondary release of TPP from them might be higher than that of tumor cells, resulting in low accumulation of TPP after 1 h of injection. Further kinetic studies are needed to clarify these issues. Future studies also need to study tumors in immunocompetent mice to understand the advantage of  $^3\text{H}$ -TPP over  $^{18}\text{F}$ -FDG in differentiating inflammation from tumor, especially in models that include tumor therapy.

Another advantage of TPP is its rapid clearance from blood.  $^3\text{H}$ -TPP exhibited very low values in blood from 10 min after injection, reflecting rapid washout from blood. Separate studies showed consistent findings.  $^3\text{H}$ -TPP blood-pool radioactivity was very low at 5 min—close to radioactivity measured in the brain tissue—suggesting that most of the  $^3\text{H}$ -TPP radioactivity had already cleared from the blood pool (18).  $^{11}\text{C}$ -Triphenylmethylphosphonium ( $^{11}\text{C}$ -TPMP) exhibited a rapid washout from blood in which  $^{11}\text{C}$ -TPMP activity peaked at 45–60 s and dropped sharply to very low values 1 min thereafter (19). The fast clearance of  $^3\text{H}$ -TPP from the blood pool is an essential feature of an imaging tracer. The blood clearance of a lipophilic cation such as  $^{99\text{m}}\text{Tc}$ -sestamibi is known to be very rapid, with a half-life of a few minutes (26). Considering that TPP may share the physiologic properties with  $^{99\text{m}}\text{Tc}$ -sestamibi, the kinetics of TPP would show some features of a blood flow agent: high early uptake and rapid blood clearance. Our next study will require detailed, dynamic analysis of TPP kinetics in living subjects. Biodistribution studies of  $^3\text{H}$ -TPP showed high accumulation in the kidneys and heart, which have a high density of mitochondria, but low uptake in other organs. Our autoradiographic images also

showed low background activity of  $^3\text{H}$ -TPP except for kidney (Fig. 3) and heart (data not shown). This tracer may also find utility in cardiac imaging applications independent of its role in cancer detection and monitoring. There is rather low  $^{18}\text{F}$ -FDG uptake in the brain that might be due to a hypometabolic cerebellum, which was an included brain specimen for the tissue biodistribution study.

An additional potential advantage of TPP over FDG is that there is no accumulation of TPP in BAT (Fig. 3). The current PET/CT studies revealed BAT as a potential cause of false-positive findings on  $^{18}\text{F}$ -FDG PET images of patients with cancer (27,28). BAT is typically deposited in the rodent's interscapular area and is metabolically active. Though glucose is not the major energy supply for BAT, glucose utilization by BAT increases during cold stimulation. Glucose transporter 4 is increased in BAT after exposure to cold (27). The mitochondria of BAT have a unique protein in their inner membrane, uncoupling protein, which provides a path for protons to return to the matrix without passing through the  $\text{F}_0\text{F}_1$  complex, leading to a drop in  $\Delta\Psi\text{m}$ , consistent with the autoradiographic finding without  $^3\text{H}$ -TPP accumulation in this study (29).

Voltage-dependent accumulation of  $^3\text{H}$ -TPP seems to be strong at the early stage of cancer proliferation. In a separate study,  $^3\text{H}$ -TPP accumulation showed parabolic change according to tumor ages in Lewis lung carcinoma nodules (18).  $^3\text{H}$ -TPP accumulation increased from day 14 to day 21 and decreased at 28 d after inoculation. At advanced stages of tumor development, lagging of vascularization behind the rapid growth of the malignant cells and resulting apoptotic or necrotic process involving collapse of the  $\Delta\Psi\text{m}$  and subsequent decrease in mitochondrial TPP accumulation may likely take place. Our next study will focus on the characteristics of TPP and FDG accumulation according to tumor size or age.

## CONCLUSION

$^3\text{H}$ -TPP is highly tumor specific, exhibiting high accumulation in tumors but minimal to no accumulation in an adjuvant inflammatory tissue and BAT. The development of radiolabeled phosphonium cations (e.g., labeled with  $^{18}\text{F}$  or  $^{11}\text{C}$ ) as a noninvasive imaging agent may serve as a new molecular voltage sensor probe to investigate the role of mitochondria in cancer with PET.

## ACKNOWLEDGMENTS

We thank Isabel Junie Hildebrandt for advice and thank David Stout, Waldemar Ladno, and Judy Edwards for their technical assistance. This work was supported in part by National Institutes of Health grants P50 CA86306, R01 CA82214, and Small Animal Imaging Resource Program R24 CA92865 and by Department of Energy contract DE-FC03-87ER60615.

## REFERENCES

- Wallace DC. Mitochondrial diseases in man and mouse. *Science*. 1999;283:1482–1488.
- Summerhayes IC, Lampidis TJ, Bernal SD, et al. Unusual retention of rhodamine 123 by mitochondria in muscle and carcinoma cells. *Proc Natl Acad Sci USA*. 1982;79:5292–5296.
- Lampidis TJ, Bernal SD, Summerhayes IC, Chen LB. Selective toxicity of rhodamine 123 in carcinoma cells in vitro. *Cancer Res*. 1983;43:716–720.
- Chen LB. Mitochondrial membrane potential in living cells. *Annu Rev Cell Biol*. 1988;4:155–181.
- Modica-Napolitano JS, Aprille JR. Basis for the selective cytotoxicity of rhodamine 123. *Cancer Res*. 1987;47:4361–4365.
- Modica-Napolitano JS, Aprille JR. Delocalized lipophilic cations selectively target the mitochondria of carcinoma cells. *Adv Drug Deliv Rev*. 2001;49:63–70.
- Gambhir SS, Czernin J, Schwimmer J, Silverman DH, Coleman RE, Phelps ME. A tabulated summary of the FDG PET literature. *J Nucl Med*. 2001;42(suppl):1S–93S.
- Mochizuki T, Tsukamoto E, Kuge Y, et al. FDG uptake and glucose transporter subtype expressions in experimental tumor and inflammation models. *J Nucl Med*. 2001;42:1551–1555.
- Kubota R, Yamada S, Kubota K, Ishiwata K, Tamahashi N, Ido T. Intratumoral distribution of fluorine-18-fluorodeoxyglucose in vivo: high accumulation in macrophages and granulation tissues studied by microautoradiography. *J Nucl Med*. 1992;33:1972–1980.
- Yamada S, Kubota K, Kubota R, Ido T, Tamahashi N. High accumulation of fluorine-18-fluorodeoxyglucose in turpentine-induced inflammatory tissue. *J Nucl Med*. 1995;36:1301–1306.
- Fossati G, Moulding DA, Spiller DG, Moots RJ, White MR, Edwards SW. The mitochondrial network of human neutrophils: role in chemotaxis, phagocytosis, respiratory burst activation, and commitment to apoptosis. *J Immunol*. 2003;170:1964–1972.
- Hamacher K, Coenen HH, Stocklin G. Efficient stereospecific synthesis of no-carrier-added 2-[<sup>18</sup>F]-fluoro-2-deoxy-D-glucose using aminopolyether supported nucleophilic substitution. *J Nucl Med*. 1986;27:235–238.
- Kimura M, Suzuki J, Amemiya K. Mouse granuloma pouch induced by Freund's complete adjuvant with croton oil. *J Pharmacobiodyn*. 1985;8:393–400.
- Gambhir SS, Barrio JR, Wu L, et al. Imaging of adenoviral-directed herpes simplex virus type 1 thymidine kinase reporter gene expression in mice with radiolabeled ganciclovir. *J Nucl Med*. 1998;39:2003–2011.
- Wu JC, Sundaresan G, Iyer M, Gambhir SS. Noninvasive optical imaging of firefly luciferase reporter gene expression in skeletal muscles of living mice. *Mol Ther*. 2001;4:297–306.
- Sands H, Gorey-Feret LJ, Cocuzza AJ, Hobbs FW, Chidester D, Trainor GL. Biodistribution and metabolism of internally <sup>3</sup>H-labeled oligonucleotides. I. Comparison of a phosphodiester and a phosphorothioate. *Mol Pharmacol*. 1994;45:932–943.
- Steichen JD, Weiss MJ, Elmaleh DR, Martuza RL. Enhanced in vitro uptake and retention of <sup>3</sup>H-tetraphenylphosphonium by nervous system tumor cells. *J Neurosurg*. 1991;74:116–122.
- Madar I, Weiss L, Izbicki G. Preferential accumulation of <sup>3</sup>H-tetraphenylphosphonium in non-small cell lung carcinoma in mice: comparison with <sup>99m</sup>Tc-MIBI. *J Nucl Med*. 2002;43:234–238.
- Madar I, Anderson JH, Szabo Z, et al. Enhanced uptake of [<sup>11</sup>C]TPMP in canine brain tumor: a PET study. *J Nucl Med*. 1999;40:1180–1185.
- Abdel-Dayem HM, Scott AM, Macapinlac HA, El-Gazzar AH, Larson SM. Role of <sup>201</sup>Tl chloride and <sup>99m</sup>Tc sestamibi in tumor imaging. In: Freeman LM, ed. *Nuclear Medicine Annual*. New York, NY: Raven Press; 1994:181–234.
- Delmon-Moineon LI, Piwnica-Worms D, Van den Abbeele AD, Holman BL, Davison A, Jones AG. Uptake of the cation hexakis(2-methoxyisobutylisonitrile)-technetium-99m by human carcinoma cell lines in vitro. *Cancer Res*. 1990;50:2198–2202.
- Mankoff DA, Dunnwald LK, Gralow JR, et al. [Tc-99m]-Sestamibi uptake and washout in locally advanced breast cancer are correlated with tumor blood flow. *Nucl Med Biol*. 2002;29:719–727.
- Ozcan Z, Burak Z, Erinc R, et al. Correlation of <sup>99m</sup>Tc-sestamibi uptake with blood-pool and osseous phase <sup>99m</sup>Tc-MDP uptake in malignant bone and soft-tissue tumours. *Nucl Med Commun*. 2001;22:679–683.
- Ishimori T, Saga T, Mameda M, et al. Increased <sup>18</sup>F-FDG uptake in a model of inflammation: concanavalin A-mediated lymphocyte activation. *J Nucl Med*. 2002;43:658–663.
- Jones HA, Cadwallader KA, White JF, Uddin M, Peters AM, Chilvers ER. Dissociation between respiratory burst activity and deoxyglucose uptake in human neutrophil granulocytes: implications for interpretation of <sup>18</sup>F-FDG PET images. *J Nucl Med*. 2002;43:652–657.
- Wackers FJ, Berman DS, Maddahi J, et al. Technetium-99m hexakis 2-methoxyisobutyl isonitrile: human biodistribution, dosimetry, safety, and preliminary comparison to thallium-201 for myocardial perfusion imaging. *J Nucl Med*. 1989;30:301–311.
- Cohade C, Osman M, Pannu HK, Wahl RL. Uptake in supraclavicular area fat (“USA-Fat”): description on <sup>18</sup>F-FDG PET/CT. *J Nucl Med*. 2003;44:170–176.
- Hany TF, Gharehpapagh E, Kamel EM, Buck A, Himms-Hagen J, von Schulthess GK. Brown adipose tissue: a factor to consider in symmetrical tracer uptake in the neck and upper chest region. *Eur J Nucl Med Mol Imaging*. 2002;29:1393–1398.
- Yu XX, Lewin DA, Zhong A, et al. Overexpression of the human 2-oxoglutarate carrier lowers mitochondrial membrane potential in HEK-293 cells: contrast with the unique cold-induced mitochondrial carrier CGI-69. *Biochem J*. 2001;353:369–375.